Modeling and Optimization of A Variable Stiffness Compliant Gripper with the Flexible Parallelogram Mechanism

Siyue Yao, Hao Yuan, Chenhao Wu, Yanjun Wang, Hao Wang, Genliang Chen, *Member, IEEE*

***Abstract*—The compliant parallel gripper has been widely applied in industrial fields, including automation assembly, agriculture, and electronics, owing to its compliance and versatility. However, stiffness modeling and optimal design of compliant grippers remain a challenge due to the nonlinear force-motion behaviors of flexible materials with large deflections. This paper presents a comprehensive approach to establishing an analytical stiffness model for the analysis and optimization of a compliant gripper. Elastic beams of arbitrary initial curved geometry form a flexible parallelogram mechanism, constituting a delicately designed planar compliant gripper with beneficial stiffness characteristics for operations including variable capability, axial and grasping decoupling, and a centrally located compliance center. Based on modeling, initial beam shapes are optimized to obtain pure or actively tuned passive compliance with a wide variation, over $100\times$ for grasping stiffness and over $500\times$ for axial stiffness. Finite element analysis and experiments based on elastic beams with distinct geometries and materials are carried out to validate the method. Finally, diverse grasping scenarios and a demonstration of the autonomous peg-into-hole task are accomplished, showcasing the performance and potential usage of the compliant gripper in industrial applications.**

***Index Terms*—Stiffness modeling, Compliant parallel gripper, Flexible parallelogram mechanism, Optimal design.**

I. Introduction

PARALLEL gripper is a pivotal component in industry due to its stable grasping format and general adaptation to various workpieces and tools, which has been widely used in autonomous assembly tasks [1]–[4]. However, commercial parallel grippers, including FESTO, ROBOTIQ, and SCHUNK [5], are rigid, susceptible to collision damages caused by unstructured environments and inevitable position and orientation errors [6], [7]. Consequently, compliance is demanded to provide adaptation [8]–[11]. Distinct tools and tasks call for variable properties of stiffness, not only to grasp various soft or fragile objects, but also to adjust stiffness during operations utilizing tools [12]–[14]. For instance, constant-force polishing expects a zero axial stiffness [15], [16]. Precision assembly as peg-into-hole requires a wide range of adjustable stiffness, a small one to avoid impact with obstacles, and a large one to overcome the resistance [17], [18]. Therefore, stiffness analysis is of great importance for compliant gripper designs.

Numerous studies have been devoted to introducing compliance into gripper design. Elastic joints are widely applied [19], [20]. Ciocarlie et al. [21] arranged springs in joints and optimized the stiffness to grasp a variety of objects. Chen and Lan [22] applied a force regulation mechanism with springs to actively adjust grasping force. Shirafuji et al. [23] utilized a tendon-driven strategy to adjust the joint stiffness. Another solution is to change the mechanical property through physical variation [24], including jamming effects and additional structures. Zhou et al. [25] proposed a continuous layer jamming, while Hou et al. [26] took advantage of coffee granules to vary stiffness. Sun et al. [27] devised a controllable jamming force mechanism, achieving 7.1-fold stiffness variation. Li et al. [28] embedded an internal flexible hinge shaft, and Chandrasekaran et al. [29] utilized an actively rotated truss structure to change stiffness. Bastien et al. [30] designed a snap-fit joint, presenting distinct stiffness. However, stiffness variation is greatly confined by the limited flexible elements.

To achieve a wider stiffness variation range, enormous efforts have been made to design grippers with holistic flexibility. Compliant mechanisms are extensively studied [31]–[34]. Zhang et al. [35] established a nonlinear optimization model considering both the workspace and stiffness. Wang et al. [36] employed a geometric representation in a topology optimization model and analyzed stiffness through finite element analysis (FEA). Besides, flexible beams, with an intrinsic compliance nature due to infinite degrees of freedom (DOFs), gain attention [37]–[39]. She et al. [40] introduced flexible beam modules to alter stiffness through deformation. Du et al. [41] and Xu et al. [42] utilized the length-altering strategy to vary the stiffness of flexible fingers. Tiziani et al. [43] adjusted the stiffness through an antagonist strategy. Takahashi et al. [44] utilized thin bending sheets as fingers to alter stiffness through passive deformation. Despite large stiffness variance, analysis and optimization are a great challenge. Chen et al. [45] and Xu et al. [46] constructed the stiffness model of a fin ray gripper by combining FEA and a neural network. Ottonello et al. [47] designed a Push-Latch gripper with flexible

This research was supported in part by the Science and Technology Commission of Shanghai Municipality under the Grant 25511104200 and the National Natural Science Foundation of China under the Grant 525B2057. (Corresponding author: Genliang Chen.)

Siyue Yao, Hao Yuan, and Chenhao Wu are with the Shanghai Key Laboratory of Digital Manufacture for Thin-Walled Structures, and the META Robotics Institute, Shanghai Jiao Tong University, Shanghai 200240, China (e-mail: sy.yao@sjtu.edu.cn; yuanhao2023@sjtu.edu.cn; g.rotrix@sjtu.edu.cn).

Yanjun Wang is with the Institute of Marine Equipment, Shanghai Jiao Tong University, Shanghai 200240, China (e-mail: yanjunwang@sjtu.edu.cn).

Hao Wang is with the Shanghai Key Laboratory of Digital Manufacture for Thin-Walled Structures, and the State Key Laboratory of Mechanical Systems and Vibration, Shanghai Jiao Tong University, Shanghai 200240, China (e-mail: wanghao@sjtu.edu.cn).

Genliang Chen is with the META Robotics Institute, and the Shanghai Key Laboratory of Intelligent Robotics, Shanghai Jiao Tong University, Shanghai 200240, China (e-mail: leungchan@sjtu.edu.cn).

hinges and varying cross-section fingers and analyzed stiffness through simplified models. Models like constant curvature and piecewise constant curvature [48], [49], smooth curvature [50], pseudo-rigid-body [51] introduce postulated conditions at the sacrifice of accuracy, while methods like piecewise linear strain [52] and FEA obtain precise results with a heavy computational burden by solving partial differential equations (PDEs). To sum up, existing modeling methods face a dilemma between accuracy and efficiency. It remains a challenge to construct an accurate and efficient stiffness model for large deflection elastic beams, assisting optimization design to meet various stiffness demands in practical industrial applications.

To this end, this paper presents a general approach to the modeling and analysis of a variable stiffness compliant gripper with flexible parallelogram mechanisms (FPM) constructed by elastic beams, which balances accuracy and efficiency with straightforward derivation. The analytical stiffness models of a curved elastic beam and the gripper are established by the discretization-based equivalent method of a redundant serial mechanism and force-motion coordination. Special characteristics, including decoupled stiffness components and a centrally located compliance center, are identified. On this basis, beam geometry is optimized to achieve the desired stiffness. FEA and experiments are applied to validate the effectiveness of the proposed approach. The main contributions include:

1) Presented a general analytical stiffness modeling method for initially curved elastic beams and compliant grippers, which balances model accuracy and computational efficiency.

2) Expressed initial beam shape based on Fourier descriptors and achieved geometry optimization for desired stiffness.

3) Proposed a planar compliant gripper with FPM possessing decoupled stiffness and a central compliance center.

4) Achieved passive compliance and an actively tuned stiffness variance range of over 500× in axial and over 100× in grasping direction, exceeding the existing maximum 70.9×.

This paper is organized as follows: scenario, mechanical design, and kinematics modeling are presented in Section II. The comprehensive procedures for the analytical stiffness modeling are established in Section III. Section IV provides the beam geometry optimization and FEA verification. Validation experiments and peg-into-hole demonstration are discussed in Section V. Conclusions are drawn in Section VI.

II. Design and Kinetostatics Modeling

A. Scenario of the Variable Stiffness Compliant Gripper

The autonomous peg-into-hole assembly task with hole-position uncertainty is to grasp a tool, drag along a given direction until reaching the hole location, and peg into it, as illustrated in Fig. 1. During the process, stiffness has to meet different requirements to ensure successful assembly.

The compliance of the gripper can be achieved by two means. One way is by pure passive compliance, which requires a small rotational stiffness and compliance center beyond the operating point to construct a Remote Center Compliance (RCC) tool [8]. This ensures the tool can be guided back to align with the hole in case of suffering inevitable position and orientation errors. Another way is by actively tuned compliance, which demands a wide stiffness range. Specifically, when the gripper pulls out the tool and pegs it into the hole by a robot arm, axial stiffness has to be large enough to withstand the resistance. Meanwhile, the rotational stiffness should be small for adjustments. In contrast, axial stiffness should be small while the tool moves along the irregular surface to prevent damage. As a result, this scenario poses a great challenge to the stiffness variance of compliant grippers.

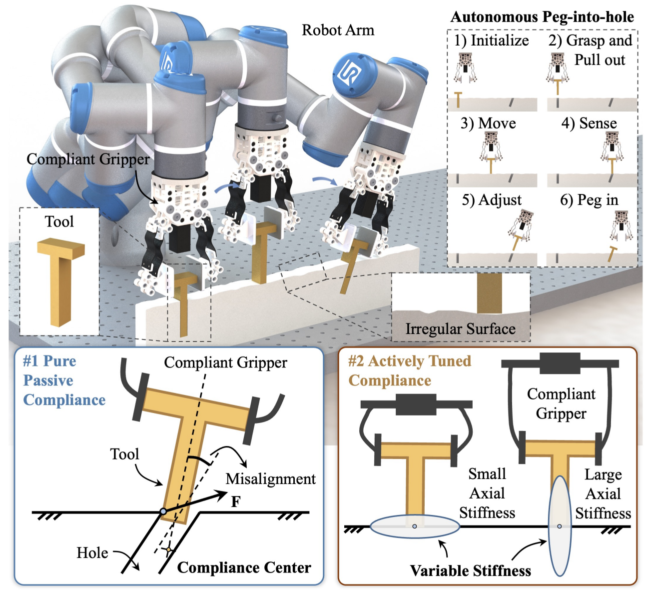

Fig. 1. Autonomous peg-into-hole scenario requiring variable stiffness.

B. Mechanical Design of the Compliant Parallel Gripper

To achieve a wide stiffness variation, a planar compliant gripper is designed with FPM. As illustrated in Fig. 2, the gripper deforms distinctively under a different actuation when grasping a tool. This lays the foundation for varying stiffness through altering actuation. Figure 2 also demonstrates the mechanical design of the compliant gripper, composed of two symmetric parallel fingers, with each one containing two parallel elastic beams. The gripper moves symmetrically, which is actuated by a single motor through slider-crank mechanisms. The arrangements and geometric parameters of the mechanism are elaborately devised to achieve a favorable force transmission and appropriate workspace. Since pure FPM, constituted by two elastic beams, deforms inconsistently, it fails to maintain parallelism under external constraints, which is detrimental to grasping. Therefore, rigid parallelogram mechanisms are additionally applied to hold parallel properties. Specifically, the two elastic beams are connected by the rigid parallelogram mechanisms at both ends to revolute joints. The proximal ends are connected to the actively actuated revolute joints, ensuring the same rotation angle for the beams. Meanwhile, the distal ends are connected to a rigid fingertip through passive revolute joints. These local parallel restrictions ensure an identical deflection for the two beams under external translational motion constraints illustrated in Sec. II-D. As a result, the gripper maintains favorable parallel and identical properties. Moreover, the intrinsic compliance of elastic beams endows an automatic centering capacity.

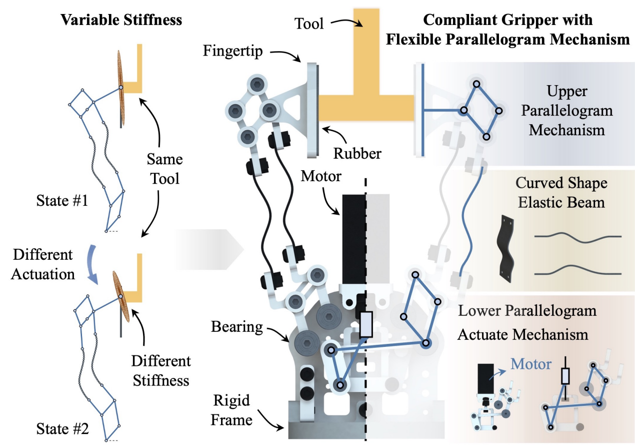

Fig. 2. Stiffness varying mechanism and mechanical design of the gripper.

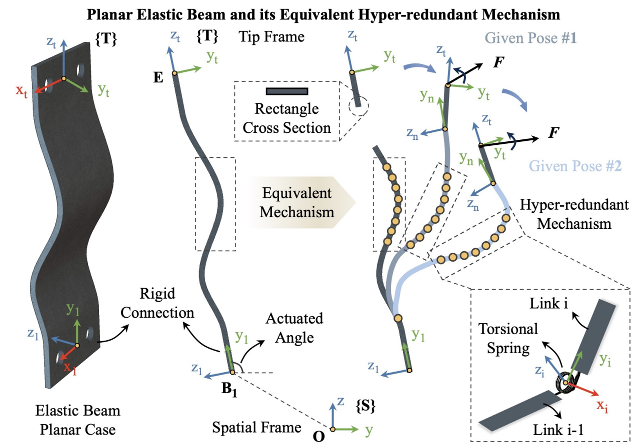

Fig. 3. Equivalent mechanism and kinetostatics model of a curved beam.

Further, FPM sets no limits to the elastic beams as long as they are identical and avoid mechanical interference. Since different geometry leads to distinct characteristics, the beam shape can be devised to satisfy desired stiffness requirements. The elastic beams adopted in this paper are made of carbon fiber (CF), PLA, or spring steel (SS) in curved shapes with a rectangular cross-section, such that the stiffness characteristics can be intentionally designed, besides being initiatively tuned.

C. Kinetostatics Modeling of a Single Curved Elastic Beam

The discretization-based method for large deflection of flexible rods, developed in prior work [53]–[55], is applied as a framework and further extended for kinetostatics analysis.

Theorem 1 (Kineto-Model)**.** *The nonlinear large deflection of a curved elastic beam can be analytically and efficiently modeled through an equivalent redundant serial mechanism.*

Proof. As illustrated in Fig. 3, the elastic beam is discretized into n relatively short segments with equal arc length. Each segment can be kinematically equal to a serial mechanism with six DOFs. For planar cases, the in-plane rotational stiffness within the plane is much smaller than the other stiffness components, leading to a further simplification for the equivalent segment as a torsional spring connecting two links, with the initial pose related to local curvature. This assumption and the consideration of shear and torsional stiffness in spatial cases are further elaborated in Text S1 in the supplementary material. Consequently, beam deformation can be characterized by the motion of an equivalent hyper-redundant multi-body system composed of rigid linkages articulated with passive torsional spring joints. The Product of Exponential formula can be used to solve the kinematics problem concisely and efficiently.

Geometric constraints are imposed at the passive revolute joint connecting the elastic beam and the upper parallelogram mechanism. Meanwhile, propagated torques are balanced through elastic joints. Construct $\{\mathrm{S}\}$ at point O on the central line of the gripper as the ground spatial frame with $\boldsymbol{x}$-axis perpendicular to the central symmetric plane and $\boldsymbol{y}$-axis along the beam length under zero actuated angle. z-axis is constructed according to the right-hand rule. $\{\mathrm{T}\}$ is the tip frame constructed at distal end E. The kinetostatic model can be integrated into a set of nonlinear algebraic equations as

$$\boldsymbol{c}(\boldsymbol{\Theta},\boldsymbol{F})=\begin{bmatrix}\boldsymbol{x}\\ \boldsymbol{\tau}\end{bmatrix}=\begin{bmatrix}\left(\log\left(\mathbf{g}_{st}(\boldsymbol{\Theta})\mathbf{g}_t^{-1}\right)\right)^{\vee}\\ \mathbf{K}_{\Theta}\boldsymbol{\Theta}-\mathbf{J}_{\Theta}^{T}\boldsymbol{F}\end{bmatrix}=\boldsymbol{0} \quad (1)$$

where $\boldsymbol{\Theta}=[\theta_1,\theta_2,...,\theta_n]^T\in\mathbb{R}^{n\times 1}$ represents joint rotation angle variables. $\boldsymbol{x}$ and $\boldsymbol{\tau}$ denote geometric and force constraints. $\mathbf{g}_{st}(\boldsymbol{\Theta})\in SE(3)$ represents the relative pose of $\{\mathrm{T}\}$ to $\{\mathrm{S}\}$ under given $\boldsymbol{\Theta}$, obtained by $\mathbf{g}_{st}(\boldsymbol{\Theta})=\exp\left(\hat{\boldsymbol{\xi}}_1\theta_1\right)\exp\left(\hat{\boldsymbol{\xi}}_2\theta_2\right)\cdots\exp\left(\hat{\boldsymbol{\xi}}_n\theta_n\right)\mathbf{g}_{st,0}$. Here, $\mathbf{g}_{st,0}$ and $\mathbf{g}_t$ are the initial and target pose, respectively. $\hat{\boldsymbol{\xi}}_i\in se(3)$ $(i=1,2,...,n)$ denote the joint twists in the initial configurations represented in 4×4 form in $\{\mathrm{S}\}$. $\mathbf{K}_{\Theta}=\mathrm{diag}(k_1,k_2,..,k_n)\in\mathbb{R}^{n\times n}$ denotes the structural stiffness matrix. k_i is the stiffness of the elastic joints. $\boldsymbol{F}\in\mathbb{R}^{6\times 1}$ represents the external force $\boldsymbol{f}$ and torque $\boldsymbol{m}$ applied at the distal end, transformed and expressed in wrench form in $\{\mathrm{S}\}$. $\mathbf{J}_{\Theta}\in\mathbb{R}^{6\times n}$ is the Jacobian matrix mapping from joint space to workspace, expressed as $\mathbf{J}_{\Theta}=[\tilde{\boldsymbol{\xi}}_1,\tilde{\boldsymbol{\xi}}_2,...,\tilde{\boldsymbol{\xi}}_n]$. $\tilde{\boldsymbol{\xi}}_i$ $(i=1,2,...,n)$ represent the joint twists under given $\boldsymbol{\Theta}$ as $\tilde{\boldsymbol{\xi}}_i=\mathbf{Ad}_{i-1}\boldsymbol{\xi}_i$. $\mathbf{Ad}_{i-1}$ denotes the adjoint transformation matrix from the first segment frame to the $(i-1)$ segment frame.

Both valid equations and independent variables are $(n+3)\times 1$ for planar cases, making the model (1) determinate. Newton-Raphson algorithm is adopted with analytically derived gradients, detailed in Text S2 in the supplementary material. □

D. Kinetostatic Modeling of the Compliant Gripper

As the flexible fingers share an identical mechanism design, the kinematics characteristic of the compliant gripper is synthesized based on those of each finger, which is analyzed through force and motion coordination relationships. As shown in Fig. 4, the pose at contact point P on the fingertip is preset. Geometric constraints are determined through rigid body motion. Benefiting from upper parallelogram mechanism, the rotation angles at distal ends, namely Q_1 and Q_2, are identical, denoted as $\gamma_1=\gamma_2=\gamma$, yet different from that at P due to revolute joint connection. Moreover, the upper parallelogram mechanism contains a two-force member, expressed as an equal but inverted force pair $\{\boldsymbol{f}_c,-\boldsymbol{f}_c\}$. The constraining and

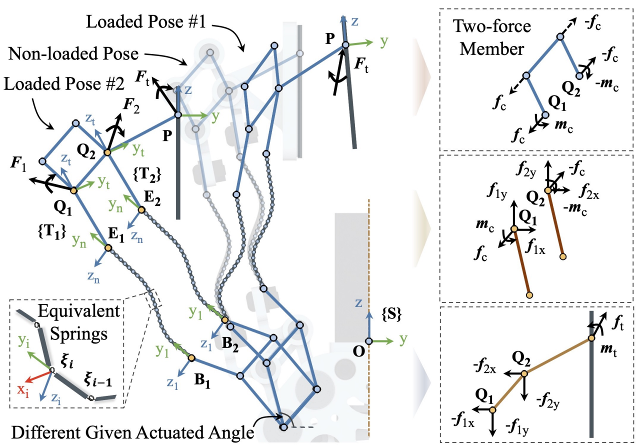

Fig. 4. Kinetostatics model of one finger based on force-motion coordination.

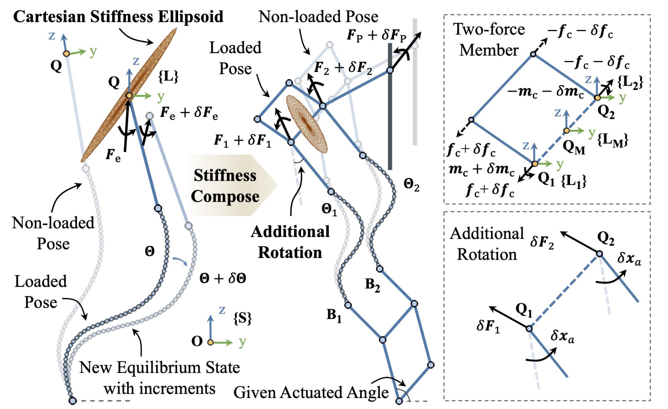

Fig. 5. Stiffness modeling from a curved elastic beam to one flexible finger.

external forces are balanced on the fingertip. Eventually, the integrated kinetostatics model can be obtained as

$$\boldsymbol{c}=\begin{bmatrix}\boldsymbol{c}_1\\ \boldsymbol{c}_2\\ \boldsymbol{c}_c\end{bmatrix}=\begin{bmatrix}\left(\log\left(\mathbf{g}_{st_1}(\boldsymbol{\Theta}_1)\mathbf{g}_{t_1}^{-1}(\gamma)\right)\right)^{\vee}\\ \mathbf{K}_{\Theta_1}\boldsymbol{\Theta}_1-\mathbf{J}_{\Theta_1}^{T}(\boldsymbol{F}_1+\boldsymbol{F}_c)\\ \left(\log\left(\mathbf{g}_{st_2}(\boldsymbol{\Theta}_2)\mathbf{g}_{t_2}^{-1}(\gamma)\right)\right)^{\vee}\\ \mathbf{K}_{\Theta_2}\boldsymbol{\Theta}_2-\mathbf{J}_{\Theta_2}^{T}(\boldsymbol{F}_2-\boldsymbol{F}_c)\\ \boldsymbol{F}_1+\boldsymbol{F}_2-\boldsymbol{F}_t\end{bmatrix}=\boldsymbol{0} \tag{2}$$

where subscript $i=\{1,2\}$ represents the two elastic beams, respectively. $\boldsymbol{c}_c$ represents the coordinated constraints. $\boldsymbol{F}_c\in\mathbb{R}^{6\times1}$ denotes the equivalent wrench of the two-force member. $\boldsymbol{F}_t\in\mathbb{R}^{6\times1}$ denotes the external wrench applied at P.

A normal case in parallel grasping is that only translational motions without rotation are imposed. Since Q_i are passive revolute joints, the only exerted torques are the equivalent torque pair $\{\boldsymbol{m}_c,-\boldsymbol{m}_c\}$ from the two-force member. Therefore, the solution can be acquired as $\boldsymbol{F}_c=\boldsymbol{0}$, $\boldsymbol{F}_1=\boldsymbol{F}_2=\frac{1}{2}\boldsymbol{F}_t$ and $\boldsymbol{\Theta}_1=\boldsymbol{\Theta}_2$, whose uniqueness is validated in Text S3 in the supplementary material. This indicates an identical deflection for the two beams, which is beneficial to parallel grasping.

III. Stiffness Modeling

A. Stiffness Modeling of a Single Curved Elastic Beam

As addressed in Sec. II-C, the equilibrium state of a single curved elastic beam can be acquired by solving (1).

Theorem 2 (Stiffness-Model)**.** *The stiffness model of a curved elastic beam can be analytically established based on the kinetostatics framework using increment analysis.*

Proof. As shown in Fig. 5, small increments near the determined balanced state are introduced to analyze the stiffness characteristics. Frame $\{\mathrm{L}\}$ is constructed at Q with axes parallel to $\{\mathrm{S}\}$. The external wrench is denoted as $\boldsymbol{F}_e$ in $\{\mathrm{L}\}$ and an increment $\delta\boldsymbol{F}_e$ is applied. As a result, the beam further deflects to a new equilibrium state where an increment of the joint variable $\delta\boldsymbol{\Theta}$ is generated. Denote $\delta\boldsymbol{F}_t$ as external wrench increment in $\{\mathrm{S}\}$. It should be noted that $\delta\boldsymbol{F}_t$ contains two components. One is the increment of exerted force. The other is the implicative increment caused by the transformation of force due to pose variance between two equilibrium states. $\delta\boldsymbol{F}_t$ can be obtained through co-adjoint transformation as

$$\begin{aligned}&\boldsymbol{F}_t=\mathbf{Ad}^*_{\mathbf{g}_{S,L}}\boldsymbol{F}_e\ \Rightarrow\ \delta\boldsymbol{F}_t=\mathbf{Ad}^*_{\mathbf{g}_{S,L}}\delta\boldsymbol{F}_e+\delta\mathbf{Ad}^*_{\mathbf{g}_{S,L}}\boldsymbol{F}_e\\ &\Rightarrow\ \delta\boldsymbol{F}_t=\delta\boldsymbol{F}_S+\mathbf{Ad}^*_{\mathbf{g}_{S,L}}\mathbf{H}_F(\mathbf{Ad}^*_{\mathbf{g}_{S,L}})^T\mathbf{J}_{\Theta}\delta\boldsymbol{\Theta}\end{aligned} \tag{3}$$

where $\delta\boldsymbol{F}_S$ denotes the transformation of the external wrench from $\{\mathrm{L}\}$ to $\{\mathrm{S}\}$. It should be noted that the rotation matrix $\mathbf{R}_{S,L}=\mathbf{I}_3\in SO(3)$ for the co-adjoint matrix $\mathbf{Ad}^*_{\mathbf{g}_{S,L}}$. The derivation of the force transformation matrix $\mathbf{H}_F$ is detailed in Text S4 in the supplementary material. Meanwhile, the relationship between $\delta\boldsymbol{\Theta}$ and $\delta\boldsymbol{F}_t$ can be deduced as

$$(\mathbf{K}_{\Theta}-\mathbf{K}_{\mathbf{J}})\delta\boldsymbol{\Theta}=\mathbf{J}_{\Theta}^T\delta\boldsymbol{F}_t \tag{4}$$

where $\mathbf{K}_{\mathbf{J}}$ reflects the influence of configuration, derived in Text S2 in the supplementary material.

The relative motion increment of the distal end expressed in $\{\mathrm{S}\}$ can be acquired as $\delta\boldsymbol{x}_S=\mathbf{J}_{\Theta}\delta\boldsymbol{\Theta}$. Combining (3) and (4), the stiffness of a single elastic beam can be deduced as

$$\delta\boldsymbol{F}_S={}^{\mathrm{S}}\mathbf{K}\delta\boldsymbol{x}_S\ \ with\ \ {}^{\mathrm{S}}\mathbf{K}=\left(\mathbf{J}_{\Theta}(\mathbf{K}_{\Theta}-\mathbf{K}_{\mathbf{J}}-\mathbf{K}_{\mathbf{T}})^{-1}\mathbf{J}_{\Theta}^T\right)^{-1} \tag{5}$$

where $\mathbf{K}_{\mathbf{T}}=\mathbf{J}_{\Theta}^T\mathbf{Ad}^*_{\mathbf{g}_{S,L}}\mathbf{H}_F(\mathbf{Ad}^*_{\mathbf{g}_{S,L}})^T\mathbf{J}_{\Theta}$ reflects the influence of the relative position on the transformation of force. □

Figure 5 demonstrates the Cartesian stiffness ellipsoid transformed to $\{\mathrm{L}\}$ at Q in a planar form with only translational components under a given configuration. The stiffness transformation between frames is ${}^{\mathrm{A}}\mathbf{K}=\mathbf{Ad}^T_{\mathbf{g}_{S,A}}{}^{\mathrm{S}}\mathbf{K}\mathbf{Ad}_{\mathbf{g}_{S,A}}$ [53], where $\{\mathrm{A}\}$ is an arbitrary frame. This provides the basis for composing stiffness matrices of different parts in one frame.

B. Stiffness Modeling of One Flexible Finger

The stiffness analysis of one flexible finger is to integrate the stiffness of two beams through force-motion coordination. Denote $\mathbf{K}_i$ $(i=1,2)$ as the stiffness matrix in $\{\mathrm{L_i}\}$ according to Sec. III-A for two beams. A small external wrench increment is applied to the fingertip, denoted as $\delta\boldsymbol{F}_P$ in $\{\mathrm{S}\}$. The finger deflects to a new equilibrium state, generating joint variable increments. Force coordination is expressed as

$$\delta\boldsymbol{F}_P=\mathbf{Ad}^*_{\mathbf{g}_1}\delta\boldsymbol{F}_1+\mathbf{Ad}^*_{\mathbf{g}_2}\delta\boldsymbol{F}_2 \tag{6}$$

where $\delta\boldsymbol{F}_i$ denotes the wrench increment at Q_i in $\{\mathrm{L_i}\}$. $\mathbf{Ad}^*_{\mathbf{g}_i}$ is the co-adjoint matrix from $\{\mathrm{S}\}$ to $\{\mathrm{L_i}\}$ $(i=1,2)$.

Motion coordination contains additional rotational increments, denoted as $\delta\gamma_i$, besides adjoint transformation due to passive revolute joint connections at Q_i. The rotational increments are identical as $\delta\gamma_1 = \delta\gamma_2$, guaranteed by the upper parallelogram mechanism as shown in Fig. 5. Denote $\boldsymbol{\delta x}_P$ as the motion increment of fingertip in $\{\mathrm{S}\}$. $\boldsymbol{\delta x}_i$ and $\boldsymbol{\delta x}_a$ represent the total and addition motion increment of the elastic beams in $\{\mathrm{L_i}\}$, respectively. It holds that $\boldsymbol{\delta F}_i = \mathbf{K}_i\boldsymbol{\delta x}_i$ for both beams. The motion coordination can be deduced and expressed as

$$\boldsymbol{\delta x}_P = \mathbf{Ad}_{\mathbf{g}_i}(\boldsymbol{\delta x}_i - \boldsymbol{\delta x}_a) \Rightarrow \boldsymbol{\delta x}_i = \mathbf{Ad}_{\mathbf{g}_i}^{-1}\boldsymbol{\delta x}_P + \boldsymbol{\delta x}_a (i = 1,2) \quad (7)$$

Along with additional rotational increments, extra constraints on torque increments are generated. Specifically, the sum of the equivalent torque, corresponding to the passive revolute joint, is zero. Therefore, the motion relationship can be acquired by solving the torque constraint using (7) as

$$\boldsymbol{e}_m^T \textstyle\sum_{i=1}^2 \mathbf{K}_i\boldsymbol{\delta x}_i = 0 \;\Rightarrow\; \boldsymbol{\delta x}_i = \mathbf{D}_i\boldsymbol{\delta x}_P \quad (8)$$

where $\boldsymbol{e}_m \in \mathbb{R}^{6\times 1}$ is the unit vector referring to the axial direction of the passive revolute joint, which is $[1,0,0,0,0,0]^T$ in this case. $\mathbf{D}_i \in \mathbb{R}^{6\times 6}$ is the synthesized motion transformation matrix, derived in Text S5 in the supplementary material.

Finally, by integrating force and motion coordination, the stiffness matrix of one flexible finger ${}^{\mathrm{S}}\mathbf{K}$ can be deduced as

$$\boldsymbol{\delta F}_P = {}^{\mathrm{S}}\mathbf{K}\boldsymbol{\delta x}_P \quad with \quad {}^{\mathrm{S}}\mathbf{K} = \textstyle\sum_{i=1}^2 \mathbf{Ad}_{\mathbf{g}_i}^{*}\mathbf{K}_i\mathbf{D}_i \quad (9)$$

Moreover, consider the parallel grasping case in Sec. II-D. Due to identical deflections, the stiffness matrices of the two beams expressed in $\{\mathrm{L_i}\}$ are the same, as $\mathbf{K}_1 = \mathbf{K}_2 = \mathbf{K}$. Denote the mid-point of Q_1 and Q_2 as Q_M and construct frame $\{\mathrm{L_M}\}$ at Q_M with axes parallel to $\{\mathrm{S}\}$.

Theorem 3 (FPM Decoupled Property)**.** *The stiffness matrix in $\{\mathrm{L_M}\}$ of the flexible finger with FPM is decoupled for its rotational and translational components in the planar case.*

Proof. It should be noted that Q_M is special since $\boldsymbol{r}_{Q_MQ_1} + \boldsymbol{r}_{Q_MQ_2} = \boldsymbol{0}$. This leads to a crucial property as

$$\mathbf{Ad}_{\mathbf{g}_{Q_M,Q_1}}^{-1} + \mathbf{Ad}_{\mathbf{g}_{Q_M,Q_2}}^{-1} = \mathbf{Ad}_{\mathbf{g}_{Q_M,Q_1}}^{*} + \mathbf{Ad}_{\mathbf{g}_{Q_M,Q_2}}^{*} = 2\mathbf{I}_6$$

Subsequently, the stiffness matrix of the finger expressed in $\{\mathrm{L_M}\}$ can be obtained, using frame transformation to (9), as

$${}^{\mathrm{L_M}}\mathbf{K} = \begin{bmatrix} -\frac{1}{2}\hat{\boldsymbol{r}}_{12}\mathbf{K}_T\hat{\boldsymbol{r}}_{12} & \mathbf{0}_3 \\ \mathbf{0}_3 & 2\mathbf{K}_T - 2\mathbf{K}_C^T\left(\boldsymbol{e}_m^T\mathbf{K}\boldsymbol{e}_m\right)^{-1}\mathbf{K}_C \end{bmatrix} \quad (10)$$

where $\boldsymbol{r}_{12} = \boldsymbol{r}_{Q_1Q_2} = \boldsymbol{r}_{B_1B_2}$ denotes the relative position of two beams, determined during design. $\mathbf{K}_T$, $\mathbf{K}_C \in \mathbb{R}^{3\times 3}$ denote the translational and coupled components of $\mathbf{K}$. Detailed derivation is provided in Text S5 in the supplementary material. It is worth emphasizing that this beneficial property holds as long as the parallel grasping restrictions are maintained. □

C. Stiffness Modeling of the Compliant Gripper

For general cases with rotational and translational motions, the stiffness matrix of the whole compliant gripper can be obtained by straightly compositing the matrices of two flexible fingers, expressed in the same frame as $\mathbf{K}_G = \mathbf{K}_{F_1} + \mathbf{K}_{F_2}$.

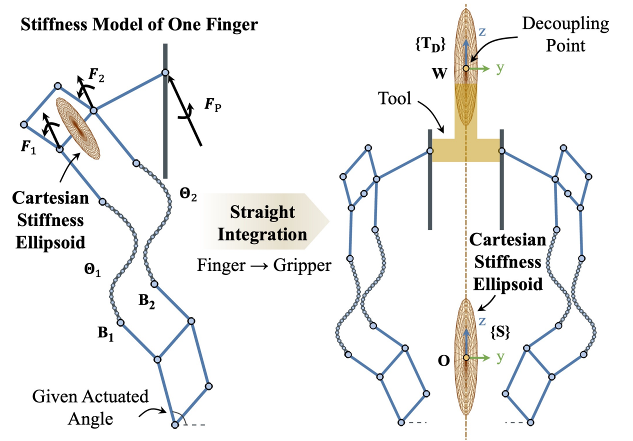

Fig. 6. Stiffness modeling of the whole compliant gripper.

Theorem 4 (Gripper Centrally Decoupled Property)**.** *The stiffness matrix of the gripper can be transformed to decouple the rotational, axial, and grasping components with a centrally located compliance center under symmetric configurations.*

Proof. Consider the specific case where the two finger configurations are symmetric according to the central line. Follow the spatial frame $\{\mathrm{S}\}$ and distal end frames $\{\mathrm{L_i}\}$ $(i = 1,2,3,4)$ constructed in Sec. III-B, force and motion relationships are consistent for two fingers due to symmetry. For instance, suppose a small translational motion increment $\boldsymbol{\delta x}_z$ imposed on one finger along z-axis arouses a force increment $\boldsymbol{\delta F}_z$. Consequently, the same increment $\boldsymbol{\delta x}_z$ imposed on the other finger will generate a force increment symmetric to $\boldsymbol{\delta F}_z$ along the central line. As a result, one fundamental property is that the stiffness matrices of two fingers possess opposite values in the coupled z-components due to symmetry. This property holds only when the stiffness matrices are expressed in frames with axes parallel and original points symmetric. For conciseness, it can be expressed in $\{\mathrm{S}\}$ in planar form as

$$\mathbf{K}_{F_1} = \begin{bmatrix} k_{xx} & k_{xy} & k_{xz} \\ k_{yx} & k_{yy} & k_{yz} \\ k_{zx} & k_{zy} & k_{zz} \end{bmatrix} \Leftrightarrow \mathbf{K}_{F_2} = \begin{bmatrix} k_{xx} & k_{xy} & -k_{xz} \\ k_{yx} & k_{yy} & -k_{yz} \\ -k_{zx} & -k_{zy} & k_{zz} \end{bmatrix} \quad (11)$$

Subsequently, ${}^{\mathrm{S}}\mathbf{K}_G$ can be expressed in $\{\mathrm{S}\}$ as

$${}^{\mathrm{S}}\mathbf{K}_G = \textstyle\sum_{i=1}^2 \mathbf{K}_{F_i} = \begin{bmatrix} 2k_{xx} & 2k_{xy} & 0 \\ 2k_{yx} & 2k_{yy} & 0 \\ 0 & 0 & 2k_{zz} \end{bmatrix} \quad (12)$$

The rotational and translational components can be further decoupled to obtain a diagonal matrix through frame transformation. Suppose k_{yy} is non-zero in a general sense. Construct frame $\{\mathrm{T_D}\}$ with axes parallel to $\{\mathrm{S}\}$ at point W located on the central line with planar coordinate $\boldsymbol{r}_{OW} = [0, -k_{yy}^{-1}k_{xy}]^T$ in $\{\mathrm{S}\}$, as depicted in Fig. 6. Through adjoint transformation, the stiffness matrix in planar form in $\{\mathrm{T_D}\}$ can be simplified as

$${}^{\mathrm{T_D}}\mathbf{K}_G = \begin{bmatrix} 2k_{xx} - 2k_{yy}^{-1}k_{xy}^2 & 0 & 0 \\ 0 & 2k_{yy} & 0 \\ 0 & 0 & 2k_{zz} \end{bmatrix} = \mathbf{diag}\{k_x, k_y, k_z\} \quad (13)$$

where k_x, k_y and k_z denote the planar stiffness components. It should be noted that the stiffness model in planar cases is established based on the kinetostatics model, neglecting the translational, torsional, and shear stiffness of the segments.

As indicated by (13), the rotational, axial, and grasping components of ${}^{\mathrm{T_D}}\mathbf{K}_G$ are completely decoupled. $\{\mathrm{T_D}\}$ is the central principal frame. In addition, the compliance center W is fixed along the central line. Therefore, the relative position of W and the operating point can be intuitively compared during assembly tasks, which benefits the pure passive compliance design. Besides, the stiffness components can be obtained directly from (13), providing great convenience for optimal design of the gripper. By devising the beam geometry, the compliance center can exceed the operating point, or a large range of stiffness variance can be achieved for actively tuned compliance, meeting the requirements of distinct tasks. □

IV. Optimization and Simulation

A. Stiffness Optimization of the Compliant Gripper

As addressed in Sec. II-B, the stiffness characteristics of the compliant gripper can be devised through initial beam geometry. Therefore, a comprehensive mathematical expression of curves based on the Fourier descriptor is applied. As illustrated in Fig. 7, a general planar arbitrary curve is depicted stretching from O to A. For conformity, a planar coordinate system is established with O being the original point, $\boldsymbol{x}$-axis from O to A, and $\boldsymbol{y}$-axis orthogonal to $\boldsymbol{x}$-axis. Moreover, the curve is normalized along the $\boldsymbol{x}$-axis. To adapt to the intrinsic properties of the Fourier expression, the curve is symmetrically rotated around $[1,0]$ and periodically extended with a period of $T=2$, forming a function $f(x)$. Subsequently, a p-order Fourier expansion can be applied to approximate $f(x)$ as

$$f^*(x) = a_0 + \textstyle\sum_{i=1}^{p} a_i \cdot \cos(i\pi x) + b_i \cdot \sin(i\pi x) \tag{14}$$

where a_0 and a_i, b_i $(i = 1,2,\ldots,p)$ are the coefficients of Fourier expansion. The function is constrained at $x = 0,1$ as

$$\textstyle\sum_{i=0}^{p} a_i = \sum_{i=0}^{p} (-1)^i a_i = 0$$

Higher orders of Fourier descriptors lead to a larger design domain, yet fiercer fluctuations. Out of manufacturing considerations, $p=2$ is applied. The influence of higher-order expansion is discussed in Text S9 in the supplementary material. The range of the optimized parameters, namely the Fourier coefficients, is determined as the curve set depicted in Fig. 7. Once the parameters are given, the curve is transformed back to the beam shape according to mechanical constraints.

Consider the process of the autonomous peg-into-hole task addressed in Sec. II-A, which can be achieved through pure passive compliance or a wide range of stiffness variance. Since the geometric parameters of beams can directly increase or decrease the equivalent stiffness by the same multiple, normalized evaluation indicators are proposed. One indicator is constructed as the ratio of the minimum and maximum values of axial stiffness. Another indicator includes the rotational stiffness under the maximum axial stiffness. The characteristic length l, as the length of the operating tool, is introduced for normalization. In addition, the RCC condition is required during optimization for pure passive compliance. Weights are

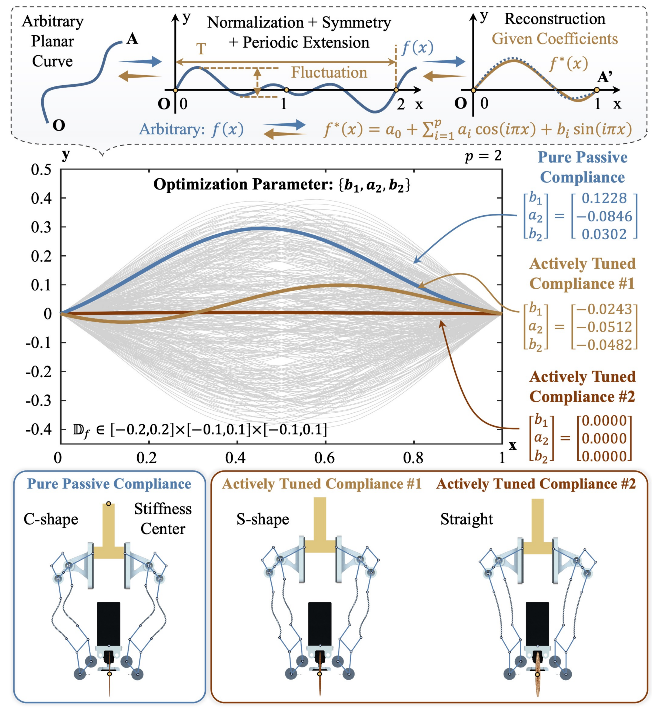

Fig. 7. Stiffness optimization procedures and optimal results.

assigned with a penalty function to construct a single-objective optimization problem, considering the design domain, actuation range, compliance center, and mechanical interference, as

$$\begin{aligned}
\min \quad & w_1 k_1^{-1} k_2 + w_2 k_1^{-1} l^{-2} k_r + \mathscr{F}\left(\mathbb{A}_f, M\right) \\
\textbf{s.t.} \quad & w_1 + w_2 = 1,\ w_i \geq 0\,(i = 1,2) \\
& \boldsymbol{c}_f \in \mathbb{D}_f \\
& \alpha \in \mathbb{A}_m \cap \mathbb{A}_f \\
& \mathscr{F}\left(\mathbb{A}_f, M\right) = \begin{cases} M & , if\ \ \mathbb{A}_f = \varnothing \\ 0 & , otherwise \end{cases} \\
& d_{\min} = \min ||\boldsymbol{q}_1 - \boldsymbol{q}_2||_2 > d_{th}
\end{aligned} \tag{15}$$

where w_i $(i = 1,2)$ denotes the assigned normalized weight. k_1 and k_2 denote the maximum and minimum value of axial stiffness, respectively. k_r denotes the rotational stiffness when axial stiffness reaches k_1. $\boldsymbol{c}_f$ denotes the Fourier coefficients in (14). $\mathbb{D}_f$ denotes the design domain of $\boldsymbol{c}_f$. α denotes the actuated angle and $\mathbb{A}_m$ is the accessible actuation range provided by the motor. $\mathbb{A}_f$ is the feasible actuation domain where the grasping force is constrained within a required range. For pure passive optimization, $\mathbb{A}_f$ additionally requires a farther compliance center than the operating point. $\mathscr{F}\left(\mathbb{A}_f, M\right)$ is the penalty function and M denotes a fairly large value. $d_{\min}$ represents the minimum distance between two beams where $\boldsymbol{q}_i$ $(i = 1,2)$ denotes an arbitrary point on each beam. d_{th} is the threshold value for preventing mechanical interference.

(15) is a unified form for both pure passive and actively tuned compliance optimization problems. Specific values for the geometric and design parameters are provided in Table S3 in the supplementary material. The classic Sequential Quadratic Programming (SQP) is applied as the iterative method for solving the constrained nonlinear optimization

TABLE I
OPTIMAL RESULTS FOR THE COMPLIANT GRIPPER DESIGN.

	Pure Passive	Actively Tuned #1	Actively Tuned #2
k_r	1.6200×10^1	6.3652×10^0	1.2568×10^3
$k_2^{-1} k_1$	1.0428	2.9823	587.82

problem. The optimal results for the corresponding ratio and rotational stiffness are listed in Table I. It should be noted that grasping force is coupled with stiffness when the actuation angle varies, and thus is considered as constraints in (15). However, it can be integrated into the objective function, aiming at devising the force variance, which is elaborated in Text S10 and Text S11 in the supplementary material.

For pure passive compliance, the optimal beam geometry is a C-type curve as demonstrated in Fig. 7. The operating point is defined by extending l from the grasping point along the central axis. Within the feasible actuation domain, z-coordinate of the compliance center alters from 185.15 mm to 261.68 mm with a range of 76.53 mm, indicating that the compliance center can reach twice the characteristic length from the grasping point. Besides, the rotational stiffness at the compliance center is 1.6200×10^1 Nm/rad under maximum axial stiffness. Although the axial stiffness variance ratio is small, only 1.0428×, it still provides some space for tuning.

For actively tuned compliance, the optimal beam geometry is close to a straight line. However, relatively small fluctuations of the curve are hard to manufacture precisely. Therefore, a straight line is utilized. The corresponding rotational stiffness is 1.2568×10^3 Nm/rad. The axial stiffness variance ratio is large, namely 587.82×. The corresponding grasping stiffness variance is 100.4×. For comparison, an additional constraint is introduced, requiring the maximum curve fluctuation to be greater than 10% of the total length. The optimal result corresponds to an S-type curve as demonstrated in Fig. 7 with a maximum curve fluctuation of 7.3768 mm. The axial stiffness variance ratio is smaller than the straight case, namely 2.9823×. However, the rotational stiffness magnitude is much smaller, making the two results possess their own advantages. As a result, a wide stiffness variance or a relatively small rotational stiffness can be achieved for the actively tuned compliance gripper design. It is worth mentioning that the design parameters only lead to the initial elastic beam shapes. The width and thickness can be further adjusted to acquire specifically desired stiffness values for the gripper.

B. FEA Validation

To validate the effectiveness of the proposed stiffness modeling method, FEA simulations are carried out. The stiffness characteristics of a single beam, one flexible finger, and the compliant gripper constituted by the three optimal types of curved beams are compared between FEA and modeled results. Initially, the optimized elastic beams are modeled in SOLIDWORKS using curves generated by the data points constructed based on Fourier descriptors. The finger and gripper are consequently modeled using the beams with simplified geometric features. Further, the models are imported into ANSYS with carbon fiber material assigned to the beams and steel to other frames. Mid-surfaces are affixed to the beams before all parts are meshed. Geometric constraints and loads are then exerted accordingly. Large deflection is utilized due to the geometric nonlinearity of the beams. Out-of-plane motions are neglected. The results are demonstrated in Fig. 8.

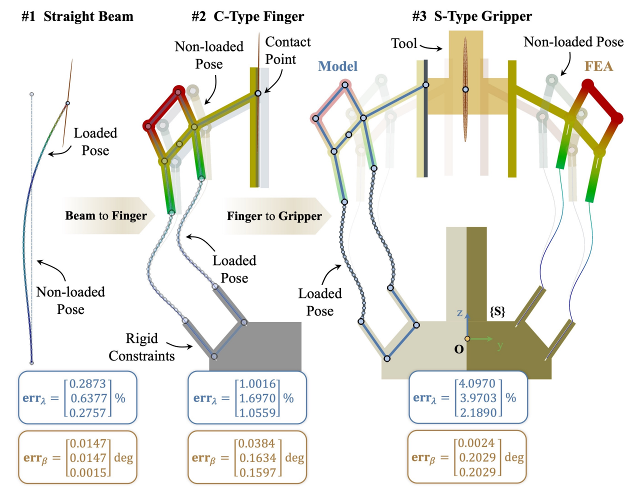

Fig. 8. FEA results compared with the modeled results.

From the results, it can be seen that all three cases, including a straight beam, one flexible finger composed of C-type curved beams, and the compliant gripper constructed using S-type curved beams, produce almost identical deformations for the modeled and simulated results. Further, both stiffness matrices of FEA and modeled results are established, where the elements are substantially consistent. The eigenvalues $\boldsymbol{\lambda}$ and eigenvectors $\boldsymbol{\beta}$ of the stiffness matrix are obtained and compared. $\boldsymbol{\lambda}$ corresponds to the principal stiffness, while $\boldsymbol{\beta}$ are related to the principal stiffness axes. The maximum errors are 4.0970% for $\boldsymbol{\lambda}$ and 0.2029° for $\boldsymbol{\beta}$, demonstrating the validity of the proposed stiffness models for a curved elastic beam, flexible finger, and compliant gripper. Detailed stiffness matrices are provided in Table S5 in the supplementary material.

V. EXPERIMENT VALIDATION

A. Experimental Setup

To further verify the proposed modeling method, experimental studies have been carried out. Figure 9 illustrates the detailed experimental setup for stiffness validation. The compliant gripper is designed according to the parameters and connected to the experimental table while grasping a tool under a given actuation. Besides, a pushing end-effector, along with an F/T sensor, is connected to a robot arm UR3 in series. The OptiTrack motion capture system is applied to acquire the relative poses and positions of the gripper and the end-effector. During the experiment, the tip end of the tool is contacted and pushed by the end-effector away from the initial equilibrium state with a small motion increment, which is controlled by the robot arm. Consequently, the actual motion increment of the tool, denoted as $\Delta \boldsymbol{x}_i$, is calculated from the coordinates of the markers fixed to the tool, which are obtained by OptiTrack. The pose of the end-effector is also acquired

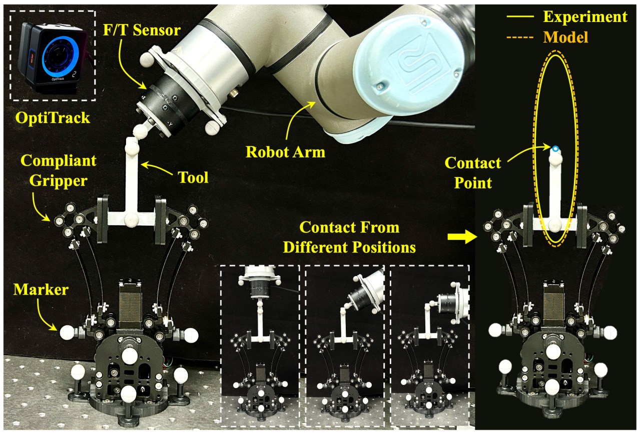

Fig. 9. Validation experiment setup and comparison with the model.

from the position measuring system. On this basis, forces and torques are recorded and then transformed to the tip end of the tool to calculate the force increment $\Delta \boldsymbol{F}_i$. The tip end of the tool is pushed with a variety of increments from various directions to construct a set of motion and force increments in planar form, expressed in matrix as $\mathbf{X} = \{\Delta \boldsymbol{x}_i\}$ and $\mathbf{F} = \{\Delta \boldsymbol{F}_i\}$. Based on the measured increments, the measured stiffness matrix $\mathbf{K}$ can thus be synthesized using the least square method and further expressed in symmetric form as

$$\mathbf{K} = \frac{1}{2}\left(\left(\left(\mathbf{X}\mathbf{X}^T\right)^{\dagger}\mathbf{X}\mathbf{F}^T\right)^T + \left(\mathbf{X}\mathbf{X}^T\right)^{\dagger}\mathbf{X}\mathbf{F}^T\right) \tag{16}$$

where $\mathbf{X}$ and $\mathbf{F} \in \mathbb{R}^{3\times m}$ including m experimental results.

B. Stiffness Model Validation

To validate the generalizability of the proposed method, grippers with elastic beams of distinct materials and geometries are tested. Four cases are targeted, including straight beams made of CF and SS, C-shape and S-shape beams made of PLA, as shown in Fig. 9 and Fig. 10. The straight beams are $0.3\,mm$ thick, whereas the C-shape and S-shape beams are $1.8\,mm$ and $1.5\,mm$, respectively, which exhibit distinct structural compliance. The composed gripper grasps a T-type tool under a given actuation angle, which alters for the four cases, leading to varying stiffness characteristics. $m = 12$ groups of motion and force increments are applied. Original test data and derived stiffness matrices are provided in Tables S7 to S12 in the supplementary material. The pose and position increments of the tip end of the tool under 12 loaded cases relative to the unloaded case for elastic beams with different materials are depicted in Fig. 11. Moreover, forces and torque are generated and compared using the derived and modeled stiffness matrices and motion increments in Fig. 11, where M_x and F_y are enlarged several times to make the comparison clearer. From the quantitative results summarized in Table II, maximum $1.8247\,N$ force and $0.1261\,Nm$ torque errors are observed for CF and PLA cases. Errors for SS beams are larger since this case possesses larger principal stiffness.

The experimentally derived and correspondingly modeled Cartesian stiffness ellipsoids are depicted in Fig. 9 for the

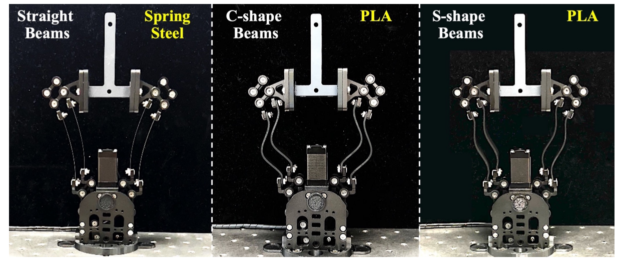

Fig. 10. Grippers with different curved beams made of distinct materials.

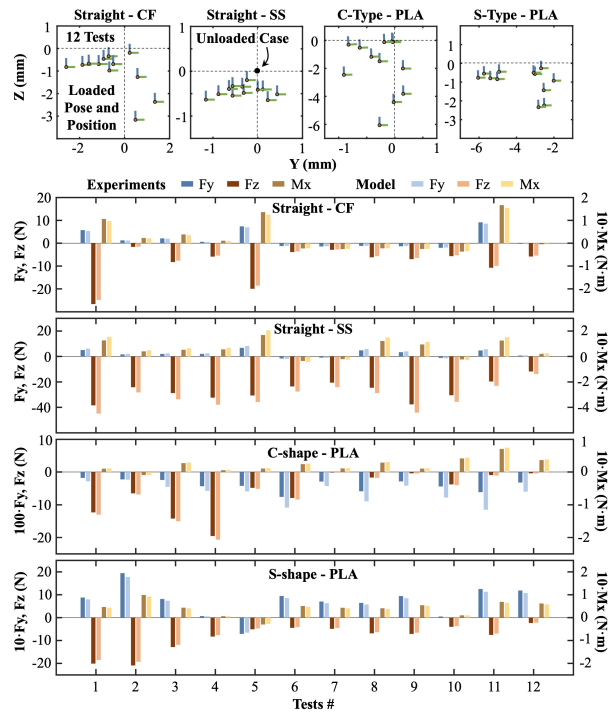

Fig. 11. Loaded configurations and force comparison with model results.

straight CF beam case with planar components to intuitively exhibit the difference. It can be seen from the results that the two ellipses align in the major and minor axial directions with only a small angular deviation. The magnitudes of the two ellipses differ by a rather close multiple, attributed to a difference between Young's modulus of the practically used CF and the model. After calibration of the Young's modulus (to $72.9280\,GPa$), the maximum errors are 6.5953% for the principal stiffness and 0.0734° for the principal axes direction. Similarly, the Young's modulus is calibrated for the other cases. From the results, all the modeled stiffness matrices align with the experimental one in principal stiffness axial directions with small angular deviations. The average and maximum errors between experiments and models are provided in Table. II, where all the principal stiffness and axes errors are less than 10% and 2°. As a consequence, the proposed method exhibits a high precision in stiffness modeling for materials and geometry in general sense, showing potential for optimal design of compliant grippers to accomplish industrial tasks.

The errors are attributed to several factors. One is the dimensional deviations when transforming physical grippers into the

TABLE II
AVERAGE AND MAXIMUM ERRORS FOR FORCE AND STIFFNESS.

Cases	Error	M_x (Nm)	F_y (N)	F_z (N)	λ (%)	β (deg)
Straight CF	Avg.	0.0380	0.1742	0.6211	6.4352	0.0724
	Max.	0.1261	0.5848	1.8247	6.5953	0.0734
Straight SS	Avg.	0.1592	0.6243	4.5638	2.1272	0.0418
	Max.	0.3665	1.4697	6.4802	2.3919	0.0493
C-shape PLA	Avg.	0.0150	0.0224	0.3604	9.3566	0.9615
	Max.	0.0385	0.0538	1.1007	9.7781	1.4337
S-shape PLA	Avg.	0.0294	0.0805	0.6639	6.7782	0.1750
	Max.	0.0665	0.1742	1.6059	7.8337	0.2592

corresponding schematic diagram of the mechanism. Besides, the stiffness matrix is synthesized based on motion and force increments in the neighborhood of the tool tip end, which is different from the model directly derived under a given configuration. In addition, the manufacturing deviations from the designed curves will cause less accuracy, especially for 3D-printed beams. Larger stiffness under distinct configurations causes less precise motion increments, while smaller ones lead to less precise force increments. For all tested cases, SS beams exhibit the least errors due to larger stiffness, despite larger values for forces and torque errors. Moreover, material properties make an effect, including better elasticity for SS and more obvious material nonlinearity for PLA.

C. Grasping and Compliance Demonstration

The grasping scenarios of the designed compliant gripper are demonstrated in Fig. 12, handling diverse objects with distinct properties, including a soft sponge, a rigid brick, a light bolt, and a heavy stone. This reveals the potential usage of the proposed compliant gripper in practical applications.

Further, a validation for the gripper with pure passive compliance is demonstrated in Fig. 13. The optimal C-shape beams are applied. The parallel grasping case is depicted, where an identical deformation of the beams can be observed. For the autonomous peg-into-hole task, several orientation and position errors are intentionally introduced by the robot arm, including a 5° orientational deviation and a further 3.5 mm positional deviation. During the pegging process, the tool overcomes these deviations and adapts to the hole passively, without active control, despite slight rotational motions being induced at the tip of the tool. Compared with rigid grippers that damage the tool due to errors, the proposed compliant gripper effectively showcases benefits in flexible assembly tasks. A detailed motion and grasping capacity, along with the peg-into-hole operation, are provided in the supplementary video.

D. Discussion

The proposed stiffness modeling and optimizing method for the compliant gripper achieves high accuracy and efficiency, showcasing potential in various scenarios with distinct optimal designs to meet different requirements, including passive compliance and actively tuned for over 500× in axial and over 100× in grasping stiffness variance, exceeding the maximum 70.9× in existing studies. Besides, the proposed modeling processes reach a computational frequency at the level of

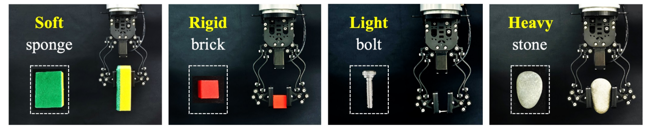

Fig. 12. Diverse grasping scenarios of the objects with different properties.

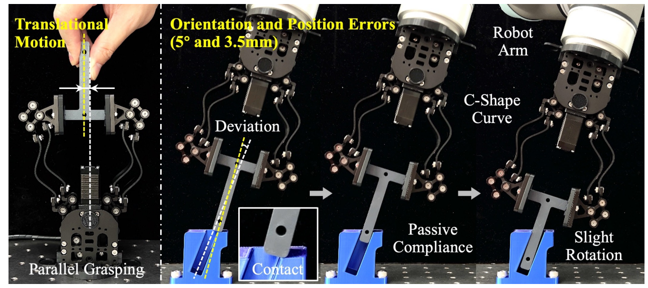

Fig. 13. Peg-into-hole demonstration based on gripper with C-shape beams.

several Hz, which shows potential in real-time control and rapid iterative design. Detailed comparisons and discussions are provided in Text S12, Text S13, Table S1, and Table S2.

However, there are limitations and room for improvement. The proposed kinetostatics and stiffness model neglects torsional stiffness for planar gripper analysis, but can be extended to spatial mechanisms with curved elastic units by integrating spatial force-motion relationships and considering the neglected stiffness components if they are of the same order, which is discussed in Text S1. It should be noted that the modeling method can analyze the nonlinear large deflections, but requires the deformation within the elastic region. The method can be further extended to a multi-DOF gripper or a multiple-finger arrangement, which may enhance and broaden the applications. Moreover, grasping force is introduced as constraints during optimization, since it changes with the stiffness for the one-DOF gripper. It can be integrated into the objective function to achieve force requirements, which is further elaborated in Text S10 and Text S11. Higher-order Fourier descriptors or other methods can be utilized to express the geometry, for which the proposed optimization is still applicable. Nevertheless, the influence on the stiffness characteristics is complicated, detailed in Text S9. Various materials can be analyzed based on the proposed method as long as the deformation is within the elastic region. A full characterization of CF has been carried out in Text S14, demonstrating its slight hysteresis and fatigue after long-term repeated loading. More comprehensive elaborations are provided in the supplementary material.

VI. CONCLUSION

In this paper, a general method is proposed for modeling, analysis, and optimization of a variable stiffness compliant gripper. The planar gripper is devised with fingers composed of FPM using curved elastic beams. Stiffness variance is achieved by adjusting the actuated angle. The main findings include presenting an analytical modeling method for curved elastic units that balances accuracy and computational efficiency. On this basis, a unified stiffness optimization framework for beam geometry is established to achieve desired characteristics. Moreover, the centrally decoupled stiffness properties of the proposed gripper are disclosed. The effectiveness and applicability of the proposed approach are validated through FEA and experiments. Eventually, an actively tuned stiffness variance of over $500\times$ in axial and over $100\times$ in grasping is achieved, which exceeds an existing maximum value of $70.9\times$. The autonomous peg-into-hole task demonstrates the capability of passive compliance based on the optimally designed compliant gripper. Diverse grasping scenarios with objects of distinct properties are displayed, showing the potential usage of the proposed gripper for various industrial scenarios.

Future research includes spatial compliant gripper design, modeling spatial elastic units with uneven cross-sections, and integrating sensing and active control. This will enhance the generality and practicability in broader applications, including fragile object grasping and precision assembly.

REFERENCES

[1] M. Cutkosky, "On grasp choice, grasp models, and the design of hands for manufacturing tasks," *IEEE Transactions On Robotics and Automation*, vol. 5, no. 3, pp. 269–279, 1989.

[2] L. Birglen and T. Schlicht, "A statistical review of industrial robotic grippers," *Robotics and Computer-Integrated Manufacturing*, vol. 49, pp. 88–97, 2018.

[3] D. Arulkirubakaran, R. Prince, R. Ramesh, T. Rajesh, K. Anand, S. Mathew, S. Baby, J. Sharon, and K. Kishore, "Evolution of industrial robotic grippers - a review," in *Recent Advances in Materials and Modern Manufacturing*, Singapore, 2022, pp. 553–563.

[4] L. Ellekilde and H. Petersen, "Design and test of object aligning grippers for industrial applications," in *2006 IEEE/RSJ International Conference on Intelligent Robots and Systems*, 2006, pp. 5165–5170.

[5] M. Honarpardaz, M. Tarkian, J. Ölvander, and X. Feng, "Finger design automation for industrial robot grippers: A review," *Robotics and Autonomous Systems*, vol. 87, pp. 104–119, 2017.

[6] G. Monkman, S. Hesse, R. Steinmann, and H. Schunk, *Robot Grippers*. John Wiley & Sons, 2007.

[7] H. Pan, S. Tang, G. Chen, and H. Wang, "Active control of contact force for a quasi-translational flexible-link parallel mechanism," *Journal of Mechanisms and Robotics*, vol. 16, no. 7, p. 071015, 2023.

[8] W. Wang, R. Loh, and E. Gu, "Passive compliance versus active compliance in robot-based automated assembly systems," *Industrial Robot*, vol. 25, no. 1, pp. 48–57, 1998.

[9] J. Hughes, U. Culha, F. Giardina, F. Guenther, A. Rosendo, and F. Iida, "Soft manipulators and grippers: A review," *Frontiers in Robotics and AI*, vol. 3, pp. 1–12, 2016.

[10] G. Chen, S. Tang, X. Duan, and H. Wang, "Design, modeling, and evaluation of parallel continuum robots: A survey," *Science China Technological Sciences*, vol. 67, p. 673–695, 2024.

[11] G. Chen, J. Luo, S. Yao, H. Yuan, Y. Wang, T. Yu, H. Wang, and Z. Lin, "Contact sensing methodology based onpropagation of interaction-induceddeformation in elastic beams," *The International Journal of Robotics Research*, pp. 1–21, 2026.

[12] L. Odhner, L. Jentoft, M. Claffee, N. Corson, Y. Tenzer, R. Ma, M. Buehler, R. Kohout, R. Howe, and A. Dollar, "A compliant, underactuated hand for robust manipulation," *The International Journal of Robotics Research*, vol. 33, no. 5, pp. 736–752, 2014.

[13] J. Shintake, V. Cacucciolo, D. Floreano, and H. Shea, "Soft robotic grippers," *Advanced Materials*, vol. 30, no. 29, p. 1707035, 2018.

[14] Z. Zhang, W. Fan, Y. Long, J. Dai, J. Luo, S. Tang, Q. Lu, X. Wang, H. Wang, and G. Chen, "Hybrid-driven origami gripper with variable stiffness and finger length," *Cyborg and Bionic Systems*, vol. 5, p. 0103, 2024.

[15] Z. Wu, X. Wang, Z. Lyu, and Q. Xu, "Design of a novel passive polishing end-effector with adjustable constant force and wide operating angle," *IEEE/ASME Transactions on Mechatronics*, pp. 1–11, 2024.

[16] T. Yan, J. Chen, S. Yao, X. Duan, Y. Wang, H. Wang, and G. Chen, "Design of a novel force-controlled end-effector with passive structural compliance and intrinsic contact sensing," *IEEE Transactions on Automation Science and Engineering*, vol. 22, pp. 23 202–23 213, 2025.

[17] C. Beltran-Hernandez, D. Petit, I. Ramirez-Alpizar, and K. Harada, "Variable compliance control for robotic peg-in-hole assembly: A deep-reinforcement-learning approach," *Applied Sciences*, vol. 10, no. 19, 2020.

[18] S. Tang, Z. Liang, Z. Zhang, X. Duan, H. Wang, and G. Chen, "A redundant parallel continuum manipulator with stiffness-varying and force-sensing capability," *IEEE Transactions on Automation Science and Engineering*, pp. 1–13, 2024.

[19] W. Chen, C. Xiong, and Y. Wang, "Analysis and synthesis of underactuated compliant mechanisms based on transmission properties of motion and force," *IEEE Transactions on Robotics*, vol. 36, no. 3, pp. 773–788, 2020.

[20] H. Choi and M. Koc, "Design and feasibility tests of a flexible gripper based on inflatable rubber pockets," *International Journal of Machine Tools and Manufacture*, vol. 46, no. 12, pp. 1350–1361, 2006.

[21] M. Ciocarlie, F. Hicks, R. Holmberg, J. Hawke, M. Schlicht, J. Gee, S. Stanford, and R. Bahadur, "The velo gripper: A versatile single-actuator design for enveloping, parallel and fingertip grasps," *The International Journal of Robotics Research*, vol. 33, no. 5, pp. 753–767, 2014.

[22] C. Chen and C. Lan, "An accurate force regulation mechanism for high-speed handling of fragile objects using pneumatic grippers," *IEEE Transactions on Automation Science and Engineering*, vol. 15, no. 4, pp. 1600–1608, 2018.

[23] S. Shirafuji, S. Ikemoto, and K. Hosoda, "Development of a tendon-driven robotic finger for an anthropomorphic robotic hand," *The International Journal of Robotics Research*, vol. 33, no. 5, pp. 677–693, 2014.

[24] H. Wei, Y. Shan, Y. Zhao, L. Qi, and X. Zhao, "A soft robot with variable stiffness multidirectional grasping based on a folded plate mechanism and particle jamming," *IEEE Transactions on Robotics*, vol. 38, no. 6, pp. 3821–3831, 2022.

[25] Y. Zhou, L. Headings, and M. Dapino, "Discrete layer jamming for variable stiffness co-robot arms," *Journal of Mechanisms and Robotics*, vol. 12, no. 1, p. 015001, 2019.

[26] T. Hou, X. Yang, Y. Aiyama, K. Liu, Z. Wang, T. Wang, J. Liang, and Y. Fan, "Design and experiment of a universal two-fingered hand with soft fingertips based on jamming effect," *Mechanism and Machine Theory*, vol. 133, pp. 706–719, 2019.

[27] X. Sun, M. Zhong, W. Chen, W. Chen, and G. Yang, "A novel variable stiffness soft gripper with optimized pneumatic actuator for robust grasping," *IEEE/ASME Transactions on Mechatronics*, pp. 1–12, 2025.

[28] X. Li, W. Chen, W. Lin, and K. Low, "A variable stiffness robotic gripper based on structure-controlled principle," *IEEE Transactions on Automation Science and Engineering*, vol. 15, no. 3, pp. 1104–1113, 2018.

[29] K. Chandrasekaran, A. Somayaji, and A. Thondiyath, "A novel design for a compliant mechanism based variable stiffness grasper through structure modulation," *Journal of Medical Devices*, vol. 15, no. 1, p. 014501, 2021.

[30] J. Bastien and L. Birglen, "Variable stiffness soft robotic fingers using snap-fit kinematic reconfiguration," *IEEE Transactions on Robotics*, vol. 39, no. 6, pp. 4567–4580, 2023.

[31] B. Zhu, X. Zhang, H. Zhang, J. Liang, H. Zang, H. Li, and R. Wang, "Design of compliant mechanisms using continuum topology optimization: A review," *Mechanism and Machine Theory*, vol. 143, p. 103622, 2020.

[32] A. Reddy, N. Maheshwari, S. Sahu, and G. Ananthasuresh, "Miniature compliant grippers with vision-based force sensing," *IEEE Transactions on Robotics*, vol. 26, no. 5, pp. 867–877, 2010.

[33] Y. She, S. Wang, S. Dong, N. Sunil, A. Rodriguez, and E. Adelson, "Cable manipulation with a tactile-reactive gripper," *The International Journal of Robotics Research*, vol. 40, no. 12, pp. 1385–1401, 2021.

[34] Z. Lyu and Q. Xu, "Design of a new bio-inspired dual-axis compliant micromanipulator with millimeter strokes," *IEEE Transactions on Robotics*, vol. 39, no. 1, pp. 470–484, 2023.

[35] R. Wang, X. Zhang, B. Zhu, H. Zhang, B. Chen, and H. Wang, "Topology optimization of a cable-driven soft robotic gripper," *Structural and Multidisciplinary Optimization*, vol. 62, p. 2749–2763, 2020.

[36] R. Wang, X. Zhang, B. Zhu, H. Li, X. Zhong, and N. Xu, "A topology-optimized compliant microgripper with replaceable modular tools for cross-scale microassembly," *IEEE/ASME Transactions on Mechatronics*, vol. 29, no. 3, pp. 2067–2078, 2024.

[37] P. Kuresangsai, M. Cole, and G. Hao, "Grasp stability and design analysis of a flexure-jointed gripper mechanism via efficient energy-based modeling," *IEEE Robotics and Automation Letters*, vol. 7, no. 4, pp. 12 499–12 506, 2022.

[38] H. Xu, X. Zhang, H. Zang, J. Lai, L. Yuan, and R. Wang, “An sma-based compliant adjustable constant force gripper for micro-assembly,” *International Journal of Mechanical Sciences*, vol. 278, p. 109430, 2024.
[39] J. Fu, Z. Yu, Q. Guo, L. Zheng, and D. Gan, “A variable stiffness robotic gripper based on parallel beam with vision-based force sensing for flexible grasping,” *Robotica*, p. 1–19, 2023.
[40] *Design and Prototype of a Tunable Stiffness Arm for Safe Human-Robot Interaction*, ser. International Design Engineering Technical Conferences and Computers and Information in Engineering Conference, vol. Volume 5B: 40th Mechanisms and Robotics Conference, 2016.
[41] X. Du, H. Mo, J. Yi, L. Huang, and L. Yin, “Hybrid compliant control with variable-stiffness wrist for assembly and grinding application,” *Robotics and Autonomous Systems*, vol. 180, p. 104756, 2024.
[42] H. Xu, L. Jiang, J. Tang, J. Pan, and W. Zeng, “Design and research of a multi-modal variable stiffness soft gripper,” *Journal of Intelligent & Robotic Systems*, vol. 111, p. 113, 2025.
[43] L. Tiziani, A. Hart, T. Cahoon, F. Wu, H. Asada, and F. Hammond, “Empirical characterization of modular variable stiffness inflatable structures for supernumerary grasp-assist devices,” *The International Journal of Robotics Research*, vol. 36, no. 13-14, p. 1391–1413, 2017.
[44] T. Takahashi, M. Watanabe, K. Tadakuma, E. Takane, M. Konyo, and S. Tadokoro, “Two-sheet type rotary-driven thin bending mechanism realizing high stiffness,” *IEEE Robotics and Automation Letters*, vol. 6, no. 4, pp. 8333–8340, 2021.
[45] G. Chen, S. Tang, S. Xu, T. Guan, Y. Xun, Z. Zhang, H. Wang, and Z. Lin, “Intrinsic contact sensing and object perception of an adaptive fin-ray gripper integrating compact deflection sensors,” *IEEE Transactions on Robotics*, vol. 39, no. 6, pp. 4482–4499, 2023.
[46] W. Xu, H. Zhang, H. Yuan, and B. Liang, “A compliant adaptive gripper and its intrinsic force sensing method,” *IEEE Transactions on Robotics*, vol. 37, no. 5, pp. 1584–1603, 2021.
[47] E. Ottonello, M. Baggetta, G. Berselli, and A. Parmiggiani, “Design and validation of a push-latch gripper made in additive manufacturing,” *IEEE/ASME Transactions on Mechatronics*, vol. 28, no. 4, pp. 2083–2091, 2023.
[48] R. Webster and B. Jones, “Design and kinematic modeling of constant curvature continuum robots: A review,” *The International Journal of Robotics Research*, vol. 29, no. 13, pp. 1661–1683, 2010.
[49] J. Shi, A. Shariati, S. Abad, Y. Liu, J. Dai, and H. Wurdemann, “Stiffness modelling and analysis of soft fluidic-driven robots using lie theory,” *The International Journal of Robotics Research*, vol. 43, no. 3, pp. 354–384, 2024.
[50] L. Odhner and A. Dollar, “The smooth curvature model: An efficient representation of euler–bernoulli flexures as robot joints,” *IEEE Transactions on Robotics*, vol. 28, no. 4, pp. 761–772, 2012.
[51] V. Venkiteswaran and H. Su, “Pseudo-rigid-body models for circular beams under combined tip loads,” *Mechanism and Machine Theory*, vol. 106, pp. 80–93, 2016.
[52] H. Li, L. Xun, and G. Zheng, “Piecewise linear strain cosserat model for soft slender manipulator,” *IEEE Transactions on Robotics*, vol. 39, no. 3, pp. 2342–2359, 2023.
[53] G. Chen, H. Wang, Z. Lin, and X. Lai, “The principal axes decomposition of spatial stiffness matrices,” *IEEE Transactions on Robotics*, vol. 31, no. 1, pp. 191–207, 2015.
[54] G. Chen, Z. Zhang, and H. Wang, “A general approach to the large deflection problems of spatial flexible rods using principal axes decomposition of compliance matrices,” *Journal of Mechanisms and Robotics*, vol. 10, no. 3, p. 031012, 2018.
[55] X. Duan, W. Yan, T. Yan, G. Chen, and H. Wang, “Kinetostatics modeling and analysis of a spherical parallel continuum manipulator,” *Journal of Mechanisms and Robotics*, vol. 17, no. 1, p. 011004, 2024.

Siyue Yao received the B.S. degree in Mechanical Engineering from Shanghai Jiao Tong University, Shanghai, China, in 2022. He is currently working toward a Ph.D. degree in Mechanical Engineering, with both the Shanghai Key Laboratory of Digital Manufacture for Thin-Walled Structures, Shanghai, China, and the META Robotics Institute, SJTU.

His research interests include flexible mechanism design, modeling and control, and mechatronics.

Hao Yuan received the B.S. degree in Mechanical Design, Manufacturing, and Automation from Shandong University, Shandong, China, in 2023. He is currently working toward a Ph.D. degree in Mechanical Engineering, with both the Shanghai Key Laboratory of Digital Manufacture for Thin-Walled Structures and the META Robotics Institute, SJTU.

His research interests include compliant mechanisms, force control, and tactile sensing in robotics.

Chenhao Wu received the B.S. degree in Mechanical Engineering from Shanghai Jiao Tong University, Shanghai, China, in 2025. He is currently working toward to M.S. degree in Mechanical Engineering from Shanghai Jiao Tong University, with both the Shanghai Key Laboratory of Digital Manufacture for Thin-Walled Structures and the META Robotics Institute, SJTU.

His research interests include robotics and control of robotic systems.

Yanjun Wang received his B.S. degree in Automotive Engineering from Nanjing University of Aeronautics and Astronautics, Nanjing, China, in 2006, M.S. degree in Automotive Engineering from Shanghai Jiao Tong University, Shanghai, China in 2009, and Ph.D. degree in Mechanical Engineering from The University of British Columbia, Vancouver, Canada in 2015. Currently, he is a research fellow in the Institute of Marine Equipment, SJTU.

His research interests include robot dynamics modelling, motion, and force control.

Hao Wang received the B.S., M.S., and Ph.D. degrees all in Mechanical Engineering from Tianjin University, Tianjin, China, in 1996, 1999, and 2002. He is currently a professor with both the Shanghai Key Laboratory of Digital Manufacture for Thin-walled Structures and the State Key Laboratory of Mechanical Systems and Vibration, SJTU.

His research interests include mechanism design, multi-body system dynamics, and robotics.

Genliang Chen (M’ 14) received B.S. and Ph.D. degrees both in Mechanical Engineering from Shanghai Jiao Tong University, Shanghai, China, in 2006 and 2014, respectively. From 2016 to 2017, He was with the Biomimetic and Dexterous Manipulation Laboratory, Stanford University, as a visiting scholar. He is currently a professor with the META Robotics Institute and the Shanghai Key Laboratory of Intelligent Robotics, SJTU.

His research interests include mechanism design, robot kinematics and dynamics.